Tailoring properties of nanostructured MoO_{3-x} thin films by aqueous solution deposition

*Katherine Inzani[1], Mohammadreza Nematollahi[2], Sverre M. Selbach[1], Tor Grande[1], Magnus Langøien Waalekalv[2], Thomas Brakstad[2], Turid Worren Reenaas[2], Morten Kildemo[2] and Fride Vullum-Bruer[1]**

[1]Department of Materials Science and Engineering, Norwegian University of Science and Technology, N-7491 Trondheim, Norway

[2]Department of Physics, Norwegian University of Science and Technology, N-7491 Trondheim, Norway

Corresponding Author

*Phone: +47-73-59-39-76; e-mail: fride.vullum-bruer@ntnu.no

Keywords

Molybdenum oxide; Nanostructured thin films; Solution processing; Optical properties

Abstract

Molybdenum oxide films are required for a large range of optical, electronic and catalytic applications, and optimal film characteristics are similarly broad. Furthermore, the layered crystal structure of MoO_3 is suited to nanostructuring, which can be adapted to enhance the film properties. Here, we present a simple, aqueous route to MoO_3 thin films and attain nanostructured morphologies by control of solution parameters. Smooth and homogeneous thin films were achieved by control of the molecular species in solution by pH. The sensitivity of film quality to pH was demonstrated with the addition of PVA to the solution, which resulted in large spherical particulates on the surface. Film thickness was adjusted from 10 to 60 nm, whilst maintaining good film quality, by changing the solution concentration. Moreover, the grain size and nanocrystallite orientation varied with solution concentration. The importance of film morphology is revealed in the compositional changes of the films during hydrogen reduction, with differences in breakdown of film coverage and growth of reduced phases. Furthermore, spectroscopic ellipsometry was used to determine the optical properties of the films. This revealed changes in the dielectric function and band gap that were dependent on the level of reduction. The nanoscale morphologies presented demonstrate the potential to precisely control film morphology, dimensions, oxygen stoichiometry and phase composition by a low-cost wet chemical route.

1 Introduction

Molybdenum oxide is renowned for its multifunctionality, being utilized in catalysis,[1] optoelectronic devices,[2–5] electrochromic coatings,[6] sensors,[7] energy storage[8,9] and other emerging technologies,[10–12] often in the form of a thin film. The electronic structure of molybdenum oxide is affected by its phase composition and oxygen stoichiometry, both of which can be adjusted to tune the electrical and optical properties.[5,9,13,14] In most cases, film morphology must also be controlled to achieve good device performance.[3,6,8,15] These factors vary widely with application. Where low-conductivity and charge carrier recombination is problematic, ultra-thin, smooth and amorphous films are utilized, for example as an anode buffer layer for optoelectronic devices.[3] Microstructures with high aspect ratios are used to enhance sensitivity to adsorbed species for sensors or to increase the surface area for catalysis.[1,16] In order to be incorporated into device manufacture, these application-tailored morphologies must be compatible with scalable and low-cost solution processes. Therefore, nanostructuring of MoO_3 should be developed within the wet chemical route.

The crystal structure of MoO_3 is unique: layers of MoO_6 corner- and edge-sharing octahedra are separated by a van der Waals gap of dispersed interactions, and oxygen sits on three symmetrically inequivalent sites, singly, doubly and triply coordinated to Mo ions. The variety of bonding environments results in differences in surface free energies with orientation, which lends itself well to nanostructuring of MoO_3 crystals. Nanosized flakes, sheets, rods, wires, walls, belts, plates, spheres and flowers have all been demonstrated by physical deposition processes.[10,12,16–20] The morphologies have been shown variously to enhance sensing properties, charge carrier mobility, field emission, photoluminescence, magnetic and electrochemical properties.[10,12,16,18,20,21] These morphology effects can be due to high crystallinity, 2D-geometries or controlled porosity. With molybdenum oxide thin films, specifications are similarly diverse. Some optoelectronic devices rely on a low root mean square (RMS) roughness to limit recombination sites, and can utilize thin amorphous films.[3] In addition, optimum thickness is dependent on the application, for example, MoO_3 is used as a hole transport layer in both organic photovoltaics (OPV) and organic light emitting diodes (OLEDs), but the former requires ultra-thin films less than 10 nm thick to keep electrical resistance low, whereas the latter can incorporate films as thick as 150 nm, exploiting the resistivity as a short circuit barrier.[14,22,23] The mechanisms taking place in MoO_3 films are not always completely understood, and, especially in emerging technologies, the ideal film structure will evolve alongside device optimization.

Alongside film morphology, additional factors that affect device operation include phase composition, crystallinity and stoichiometry.[9,14,24–27] Some of these behaviours are not well understood. Stoichiometry in particular plays an important role in many applications, and the presence or absence of oxygen vacancies is critical to several devices.[5,22,25,27] Despite this, films of MoO_x can be incorporated without knowledge of the stoichiometry or even the composition and species present.[28–31] Changes in chemical bonding will obviously affect the properties of the films, and better understanding of the chemistry resultant from solution processing is necessary to controllably apply these films.

Nanoscale control of morphology is currently achievable through physical processing means, commonly vacuum evaporation, sputtering and pulsed laser deposition.[9,14,22,24,32] With atomic layer deposition, control of MoO_3 film thickness on the nanoscale has been achieved, with similar control of the growth in related chemical vapour deposition-type conditions.[33] Wet-chemical routes have the advantage of deposition in ambient conditions and low equipment costs. Furthermore, solution processing is often compatible with existing device manufacture

such as organic photovoltaics. Previously, several solution routes to MoO_3 films have been used. Oxomolybdate precursors in aqueous solution have been used to provide molybdate based ultra-thin and low roughness films which have been comparable to evaporated films, despite that in most cases the films are discontinuous or have an undetermined composition.[28,30,34,35] Another route is via dissolution of molybdenum in hydrogen peroxide, which has resulted in thick nanocrystalline films, though also not continuously covering the substrate.[1,6] A recent synthesis involved dissolving MoO_3 ammonia solution, providing nanoplates whose concentration can be increased to provide a homogeneous film.[3] These films were used for investigation of the hole injection property in organic electronics, and the discontinuous film was found to give the best device performance. Templates have been used to provide ordering in the form of mesoporous films, but in general solution processing has failed to provide control of nanostructuring of MoO_3.[8]

Here, we present an investigation into nanostructuring of solution processed MoO_3 films and produce an aligned nanocrystallite thin film morphology via a simple solution route. We demonstrate control of morphology, thickness, crystallinity and phase composition by solution parameters and post-deposition annealing. Morphology and thickness, and hence electrical and optical properties, are controlled by standard solution properties such as pH and concentration. The changing morphology results in a change in the mechanism and kinetics of reduction. This is of importance when considering reduced MoO_3 films for use in optoelectronic devices.

2 Experimental Details

2.1 Synthesis route and reduction

Solution and film preparation was done in an ISO7 cleanroom (NTNU NanoLab). Solutions for spin-coating films were made by dissolving ammonium heptamolybdate tetrahydrate ($(NH_4)_6Mo_7O_{24}\cdot 4H_2O$, referred to as AHM, 99.98% trace metals basis, Sigma-Aldrich) in deionized water to concentrations of 0.1-1 mol [Mo] L^{-1}. To prevent precipitation of MoO_3, the solution was adjusted to pH 10 by adding ammonia solution. In some cases, an aqueous solution of 6 wt.% poly(vinyl alcohol) (PVA) was added to increase the viscosity. Solutions were stirred on a hotplate at 50 °C for 30 min and then sonicated for 10 s for degassing. Quartz substrates (Spectrosil® synthetic fused silica, UQG Optics) were prepared by cleaning in ethanol and activating the surface with a 5 minute oxygen plasma treatment. (Diener Electronic, FEMTO Plasma Cleaner). The films were prepared by spin coating, applying the solutions to the substrates through a syringe with a 0.2 μm filter (Acrodisc, Pall) and spin coating at 2500 rpm for 1 minute (Laurell WS-400B-6NPP-Lite Spinner). Heat treatment of the films was done in a rapid thermal processing furnace (RTP, Jipelec JetFirst 200 Processor). A heating rate of 6 Ks^{-1} was used and the films were held at 400 °C for 10 min in an oxygen flow of 200 sccm. Multiple layers were added to the heat-treated films by the same route. For reduction of the films, RTP was done in 5 % H_2-95 % Ar flow of 1000 sccm, holding at 200 – 500 °C for 30 minutes.

2.2 Characterization

X-ray diffraction (XRD) was used to determine the phase composition of the films. A Bruker D8 Advance DaVinci X-ray Diffractometer with LynxEye™ SuperSpeed Detector was used with a CuKα radiation source in grazing-incidence geometry (grazing angle fixed at 1°, 0.03° step size, 3.2 s step time and 10° to 60° 2θ). Atomic force microscopy (AFM, Veeco diMultimode V, Nanoscope software), used to observe film morphology, was performed with Peak Force Tapping™ in ScanAsyst mode. Film thickness was measured by profilometry

(Veeco Dektak 150), with a resolution of 6 nm, after etching a step to the substrate with a 0.05 M NaOH solution. Scanning electron microscopy (FEG-SEM, Zeiss Ultra 55 Limited Edition, 10 kV) was carried out to observe the homogeneity of films over a large area. This required films to be coated with a thin layer of carbon to prevent charging. X-ray photoelectron spectroscopy (XPS) was used to determine the oxidation states present after reduction. This was obtained with a Kratos Axis Ultra with monochromatic Al Kα X-ray source with a pass energy of 20 eV. Background modelling and subtraction, peak fitting, and quantification of the components were processed using CasaXPS software. Further details are given in supplementary information SI.1.

Spectroscopic ellipsometry (SE) measurements were performed on a J. A. Woollam Co. RC2 ellipsometer. The spectral range was 210-1690 nm (photon energy range 0.73-5.9 eV) at an angle of incidence 55-75°, with 5° intervals. Transmittance measurements of the substrate were also carried out with the ellipsometer and used to develop the SE model. Briefly, the parametric dispersion model consisted of two Tauc-Lorentz oscillators for describing the dielectric function above the band gap, one Gaussian for absorption below the band gap, and a Drude oscillator for free carrier contribution at low photon energies.[36,37] A roughness layer was modelled by Bruggeman effective medium theory.[38] Details of the optical model are given in supplementary information SI.2. The refractive index, film thickness and band gap were extracted from this, and agreement between the model and measured spectra was quantified by the mean squared error (MSE).[39]

3 Results and discussion

A molybdenum oxide film as-deposited from 0.1 mol [Mo] L^{-1} solution was shown to be amorphous by XRD, and no crystallinity was detected on thermal annealing up to 300 °C in oxygen (Figure 1). Thermal annealing at 400 °C revealed the formation of crystalline MoO_3 in the film. The intensities of the Bragg reflections, however, did not correspond well with the MoO_3 reference, and only the (020), (040) and (060) planes displayed clear reflections. This strongly indicates that a preferred crystal orientation of MoO_3 formed during the crystallization of the films.

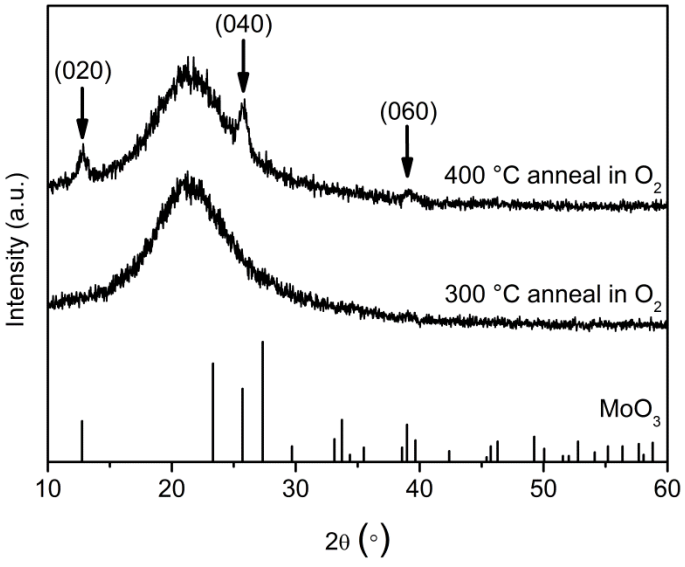

Figure 1. Grazing-incidence XRD of deposited films after annealing in oxygen in at 300 °C and 400 °C, and XRD reference for MoO_3 (PDF 00-005-0508). The (020), (040) and (060)

reflections of MoO_3 are labelled for the film annealed at 400 °C. The large amorphous background is attributable to the quartz substrate.

As seen by AFM imaging in Figure 2a, the as-deposited amorphous film covers the substrate homogenously. This can partly be attributed to the solution chemistry of the Mo^{6+} ion, which exists in the form of monomeric or polymeric oxo-ions, dependent on the pH and the concentration. The applied precursor AHM readily dissolves in water under the formation of the $Mo_7O_{24}^{6-}$polyanion.[40] The pH of AHM in aqueous solution lies between 5 and 6, caused by the partial deprotonation of NH_4^+. Further lowering of the pH results in the formation of $Mo_8O_{26}^{4-}$ ions and finally in the precipitation of MoO_3. Raising the pH, however, causes the formation of monomeric MoO_4^{2-} ions.[40] The application of a high pH solution containing monomeric MoO_4^{2-} ions during spin coating prevents the risk of uncontrolled precipitation of MoO_3 in solution upon evaporation of the solvent. The monomeric oxomolybdate species are deposited on the substrate, providing a high quality film without inclusions.

Despite the lack of long range order after 300 °C annealing (XRD), morphology changes did occur at this temperature, evidenced by AFM (Figure 2b). There appears to be clustering of nanoparticles, although homogeneous coverage is maintained across the surface. The morphology is very different after 400 °C annealing, and the film has a multicrystalline grain-like arrangement (Figure 2c). The "grains" consist of platelet-like nanocrystallites, aligned in a pattern stacked from the centre of the grain and radiating outwards until intersecting alternatively oriented nanocrystallites of the neighbouring grain. The length of the plates is in excess of 100 nm and can be up to 1 μm. At the central point, a stepped arrangement reveals the plate edges. The height of the plates was determined by taking samples of line profiles and averaging the height difference in one step (Figure 2d, with line profiles given in supplementary information SI.3). This gave an average height of 5 Å ± 2 Å. This value is of the order of one layer in the layered crystal lattice of MoO_3 (Figure 2e) which is just less than half the unit cell height and equal to 6 Å.[41] Thus, it is likely that the exposed faces of the planes are the (020) planes of the lattice. This is justified by the lower surface energy of this face, intuitive from the fact that no Mo–O bonds are broken, and the strong {020} reflections seen by XRD.

Line profiles from the central part of a grain to its edges are given in the supplementary information (SI.4). The grain height increases from the central part to the edges of the grain, with a height difference of roughly 0.4-1 nm per 100 nm. This indicates that there is stacking from the centre to the edge of the grain, but the small height difference compared to the 6 Å layer height suggests that this stacking is not level with the surface.

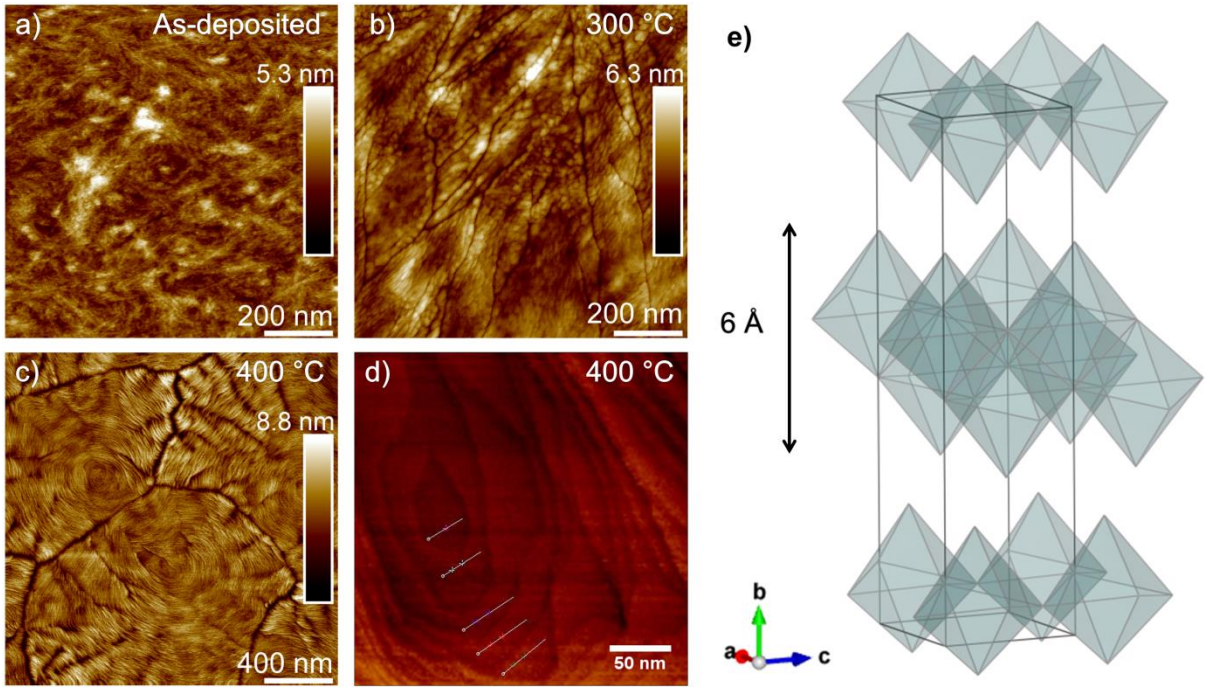

Figure 2. AFM images of films deposited from a 0.1 mol [Mo] L^{-1} AHM solution. a) As-deposited film. Films after heat treatment in O_2 at, b) 300 °C and c) 400 °C. d) Sampling of line profiles to obtain nanocrystallite step height. e) The layered crystal structure of orthorhombic MoO_3, with the layer height of 6 Å indicated.

Despite this nanostructuring, the films maintained full coverage of the substrate, and no large precipitates formed disrupting the continuity of the film. The films were smooth with an RMS roughness (Rq) of 0.85 nm, which is comparable to previously published values of amorphous films and is suitable for OPV applications. The film thickness was 10 nm, which is appropriate for the thinnest MoO_3 film applications. In order to obtain thicker films, the concentration of the deposition solution was increased. The annealing conditions were kept the same in all cases. The film thickness increased with increasing concentration in the solution, shown in Table 1. In addition, the average grain size decreased and Rq values increased with increasing concentration, also shown in Table 1. The decrease in grain size indicates that films are formed by heterogeneous nucleation and a higher nucleation rate occurs in formation of the thicker films. The orientation of the nanocrystallites also varies with film thickness (Figures 3 and 5). Low concentrations result in the concentric and stepped alignment of plates. Whereas with higher concentrations, the majority of grains consisted of

closely packed nanocrystallites oriented with {020} planes perpendicular to the surface. This change in nanocrystallite alignment can account for the increased Rq in the thicker films.

Table 1. MoO_3 films with deposition solution concentration, film thickness, average grain size and root mean square roughness values measured by AFM over a 10 μm x 10 μm area.

Solution concentration [mol [Mo] L^{-1}]	Film thickness [nm ± 5 nm]	Average grain size [μm ± 0.1 μm]	RMS roughness, Rq, [nm]
0.1	10	1.2	0.85
0.2	20	1.0	0.94
0.5	60	0.6	1.53
1.0	100	0.3	3.32

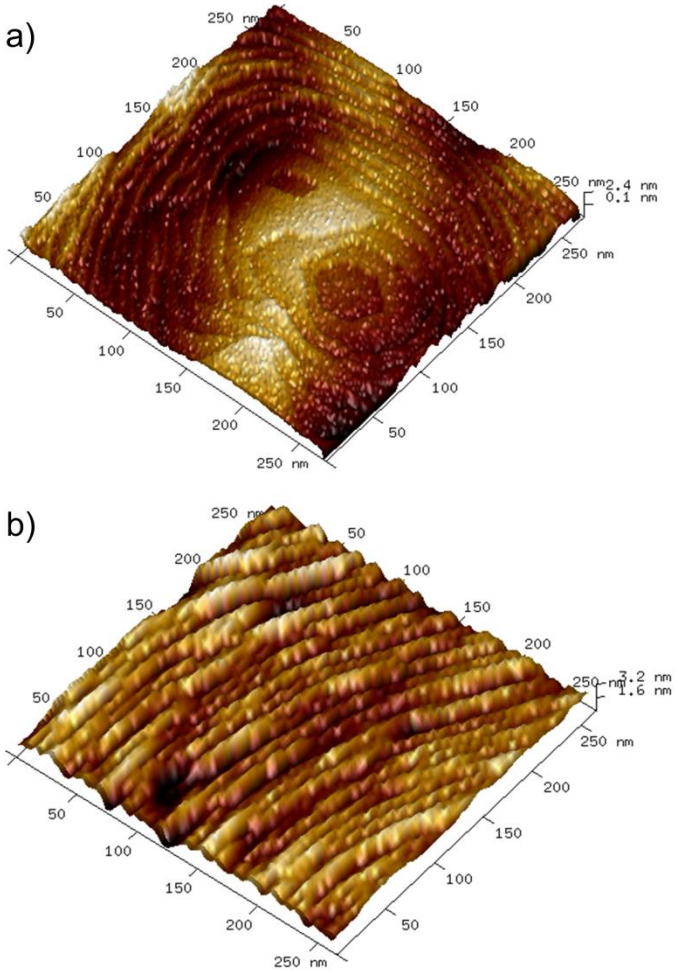

Figure 3. AFM images of, a) nanostructured stepped plates in a 0.1 mol [Mo] L^{-1} deposition film, and b) oriented nanocrystallites in a 0.5 mol [Mo] L^{-1} deposition film.

Although the 100 nm films would be applicable to many applications where thicker films are required, high concentrations (≥ 0.75 mol [Mo] L^{-1}) resulted in precipitates in the solution or deposition stage. As a result, this gave a worsened film quality with particulates on the surface. The 0.5 mol [Mo] L^{-1} solution retained a good film quality and so it was the maximum concentration used for further film depositions. Alternative methods to increase the film thickness were attempted, including multiple layer depositions, and the addition of PVA

solution to increase the viscosity. Multiple layers without the PVA additive had a negligible effect on film thickness. The addition of PVA does not alter the film quality, as shown in the homogeneous film surface scanning electron micrograph in Figure 4a, nor does it have an effect on thickness. However, multiple layers with PVA additive resulted in the appearance of micron sized spheres distributed across the surface, seen in the SEM image of a film with three layers deposited, Figure 4b.

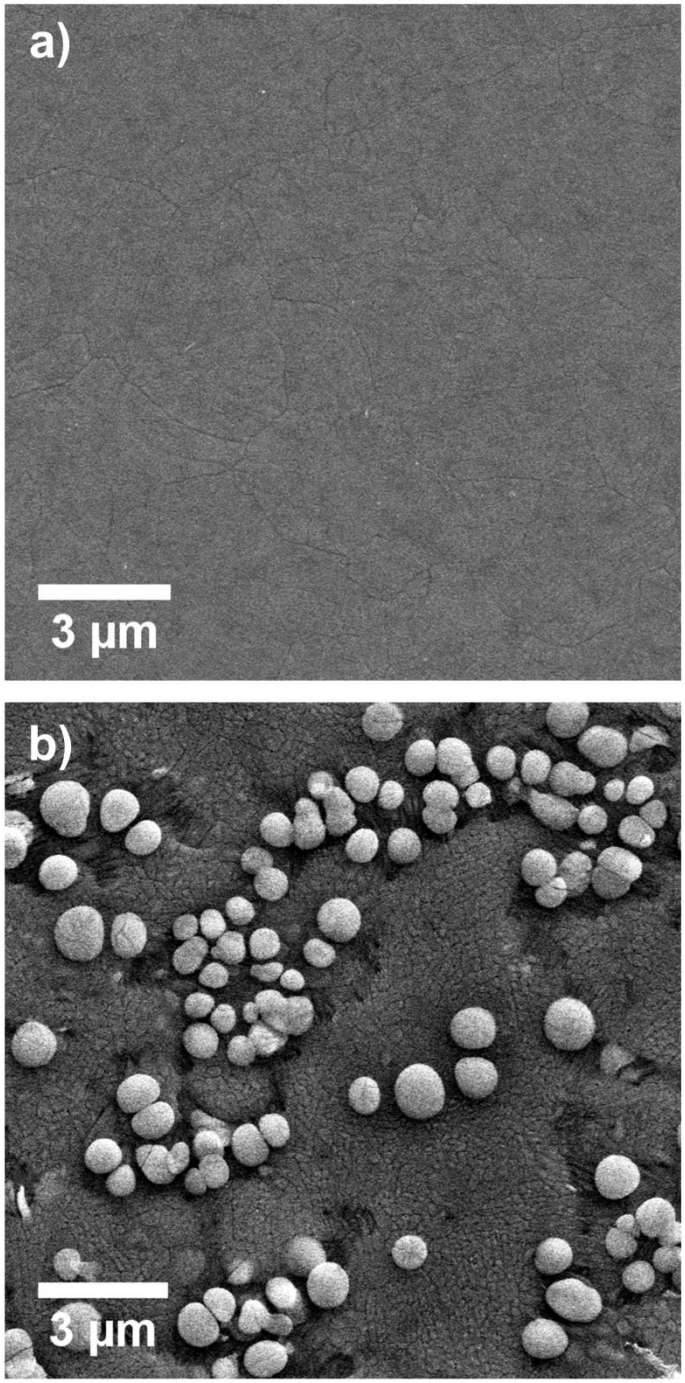

Figure 4. SEM micrographs of MoO_3 films with PVA additive, a) 1-layer deposition and b) 3-layer deposition.

The spheres are thought to be formed in solution after only a few hours ageing at room temperature. The oxomolybdate species tend to form large clusters at the low pH provided by

the PVA molecules.[42] Another possibility is that the spheres form on the surface during deposition, on contact with the acidic MoO_3 surface of prior depositions. An alternative non-acidic additive for higher viscosity might limit this problem, but the acidic MoO_3 surface could still cause precipitation. Thus, single layer deposition was all that was required for optimum film quality and no additives were found necessary.

Post-treatment in a reducing atmosphere was performed to assess the effect of hydrogen reduction on films with minimum and maximum thickness. Films from 0.1 mol [Mo] L^{-1} and 0.5 mol [Mo] L^{-1} solutions were heated under a 5% H_2 / 95% Ar flow. Changes to the film morphology are shown in the AFM images in Figure 5.

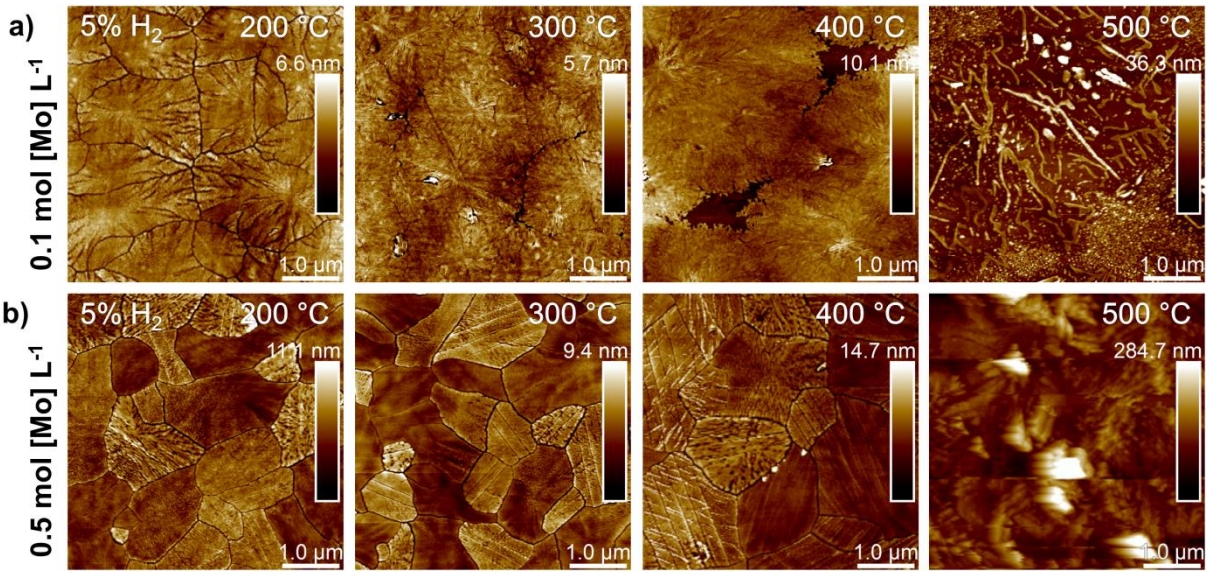

Figure 5. AFM images of MoO_3 films from a) 0.1 mol [Mo] L^{-1} solution and b) 0.5 mol [Mo] L^{-1} solution after reduction in 5% H_2 / 95% Ar gas at 200 °C, 300 °C, 400 °C and 500 °C.

The grain structure is not affected in either of the film series at 200 °C post-treatment. At 300 °C treatment of the 0.1 mol [Mo] L^{-1} deposited film, the substrate is exposed at the grain boundaries. In addition, inclusions are seen within the film, which are likely nuclei of reduced molybdenum oxide phases. The 0.5 mol [Mo] L^{-1} deposited film does not show these changes at 300 °C reduction. Increasing to 400 °C, the 0.1 mol [Mo] L^{-1} deposited film has large areas of substrate exposed and dendritic phase growth is seen. In contrast, the 0.5 mol [Mo] L^{-1} deposited film remains intact and accommodates nuclei and plate like growth of reduced phases. At 500 °C, the 0.1 mol [Mo] L^{-1} deposited film has completely disintegrated and provides very little coverage of the surface. The 0.5 mol [Mo] L^{-1} deposited film exhibits large crystal growth and has a rough and inhomogeneous surface, which made it difficult to obtain a clear image by AFM.

XPS was done to assess the degree of reduction of the films. XPS spectra of the 0.1 mol [Mo] L^{-1} and 0.5 mol [Mo] L^{-1} depositions after reduction at 400 °C are shown in Figure 6. Deconvolution of the Mo 3*d* peaks revealed the relative content of the Mo oxidation states, displayed with binding energy and FWHM in Table 2. There is a high proportion of Mo^{6+} in the 0.5 mol [Mo] L^{-1} film (91 %), which suggests that the film remains mainly MoO_3. The remainder of Mo is Mo^{5+}. In the thinner 0.1 mol [Mo] L^{-1} film, only 61 % of the Mo exists as Mo^{6+}. There is a greater proportion of Mo^{5+} (31 %) in the 0.1 mol [Mo] L^{-1} film compared to the 0.5 mol [Mo] L^{-1} film. Mo^{5+} may be present due to oxygen vacancies or as Mo_4O_{11}, Mo_9O_{26} or $Mo_{18}O_{52}$ phases. It is unlikely that Mo^{5+} is a result of hydrogen doping, as atomic

hydrogen would need to be dissociated, for example by a noble metal catalyst.[43] Without a catalyst, the reduction mechanism in hydrogen environment is known to progress through oxygen vacancy formation and reduced phase growth.[44,45] The concentration of isolated vacancies is expected to be small, as the formation of extended defects and reduced phases is favoured beyond $MoO_{2.999}$.[46]

About 8 % of the Mo in the 0.1 mol [Mo] L^{-1} deposited film is Mo^{4+}, which could be present as MoO_2. The presence of MoO_2 in the 0.5 mol [Mo] L^{-1} deposited film is ruled out as there is no Mo^{4+} detected. There is no Mo^0, Mo^{2+}, or Mo^{3+} present in either of the films. The presence of Mo^{4+} and the higher concentration of Mo^{5+} in the 0.1 mol [Mo] L^{-1} deposited film reveal that it is reduced more rapidly than the 0.5 mol [Mo] L^{-1} deposited film.

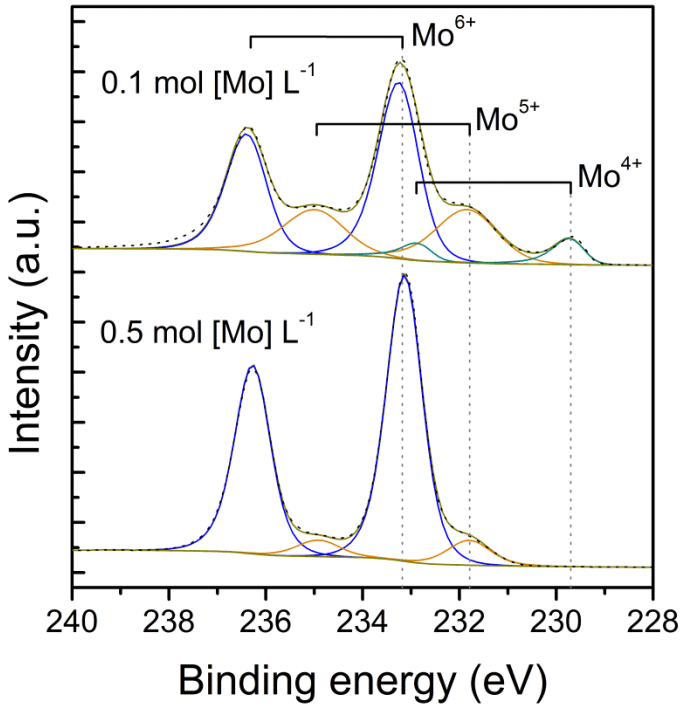

Figure 6. XPS spectra of Mo 3*d* of two film thicknesses, 0.1 mol [Mo] L^{-1} and 0.5 mol [Mo] L^{-1} depositions, after hydrogen reduction treatment at 400 °C.

Table 2. Spectral fitting parameters for Mo $3d_{5/2}$ binding energy (eV), FWHM value (eV), and the relative content of 4+, 5+ and 6+ oxidation states of Mo (%). The distribution of oxidation states of molybdenum is found from deconvolution of both Mo $3d_{5/2}$ and Mo $3d_{3/2}$.

Film deposition [mol [Mo] L^{-1}]	**Mo^{4+}** Eb [eV] FWHM [eV] Content [%]	**Mo^{5+}** Eb [eV] FWHM [eV] Content [%]	**Mo^{6+}** Eb [eV] FWHM [eV] Content [%]
0.1	229.67 0.66 8 %	231.77 1.45 31 %	233.22 0.96 61 %
0.5	- - -	231.79 1.04 9 %	233.13 0.87 91 %

The two series of films from 0.1 mol [Mo] L^{-1} and 0.5 mol [Mo] L^{-1} depositions with hydrogen reduction from 200 – 450 °C were further investigated by SE to understand the evolution of optical properties at different stages of reduction. Key parameters for the SE model and typical measured and fitted N, S, and C values are given in the supplementary information (SI.5 and SI.6). The model provided a good match to the measured transmittance (supplementary information SI.7).[47–52] The transmittance spectra are also in keeping with other reports from literature, and the transmittance generally decreases with increasing reduction.[27,53–55] The total thickness of the films matches well to the thickness obtained by profilometry and the optical band gap of the non-treated sample is in good agreement with other observed values in the 3.2 eV region for MoO_3 (SI.5).[47,48,56,57]

The dielectric function provides further insight to the phases introduced by reduction, especially for reduction temperatures above 400 °C (Figure 7). The shape of the dielectric function is similar for all of the 0.5 mol [Mo] L^{-1} deposited films up to reduction temperature 350 °C, showing a mostly transparent region up to the band gap (figures 7c and 7d). This indicates that the films are mainly MoO_3 with few oxygen vacancies as they have almost no sub-band gap absorption. The same is true for the 0.1 mol [Mo] L^{-1} deposited films but only until the reduction temperature 200 °C (figures 7a and 7b). The very small contributions from the Gaussian, only 0.05-0.10 amplitude (SI.5), could be due to small concentrations of defects. At higher temperatures, the large contribution from the Gaussian indicates the presence of intermediate phases due to the position of their absorption bands, such as Mo_4O_{11} (1.3 eV, 2.13 eV and 2.42 eV) and Mo_9O_{26} (2.12 eV), or MoO_2 (2.48 eV).[57] With the films from 0.1 mol [Mo] L^{-1} solution reduced at 350 °C, 400 °C and 450 °C, the higher amplitude at ~1.2 eV shows that there is a greater proportion of intermediate phases present in these films. This is in good agreement with the XPS results. Only the samples reduced at the highest temperature (450 °C) had significant contributions from free carriers at low photon energies. This is modelled by a Drude contribution and clearly indicates a metallic behaviour, most likely synonymous with the presence of MoO_2.[36,55]

Comparing ε_2 between the series (Figures 7b and 7d), the more reduced samples of the 0.1 mol [Mo] L^{-1} deposited films have a higher dielectric function, again indicating that this series is more sensitive to reduction and evolve a greater proportion of reduced phases.

The evolution of reduced phases is in agreement with a previous work on the progression of reduction of MoO_3.[58] It should be noted that the band gaps given by the Tauc analysis in the

previous work include the contributions from the sub-band gap states, such that the Tauc band gap decreases with the onset of reduced phases. Here, the optical analysis accounts for the sub-band gap states with the Gaussian oscillator. Quantifying these reduced phases with ellipsometry would need further analysis, as polaron absorption has also been reported at approximately 1.4 eV.[54]

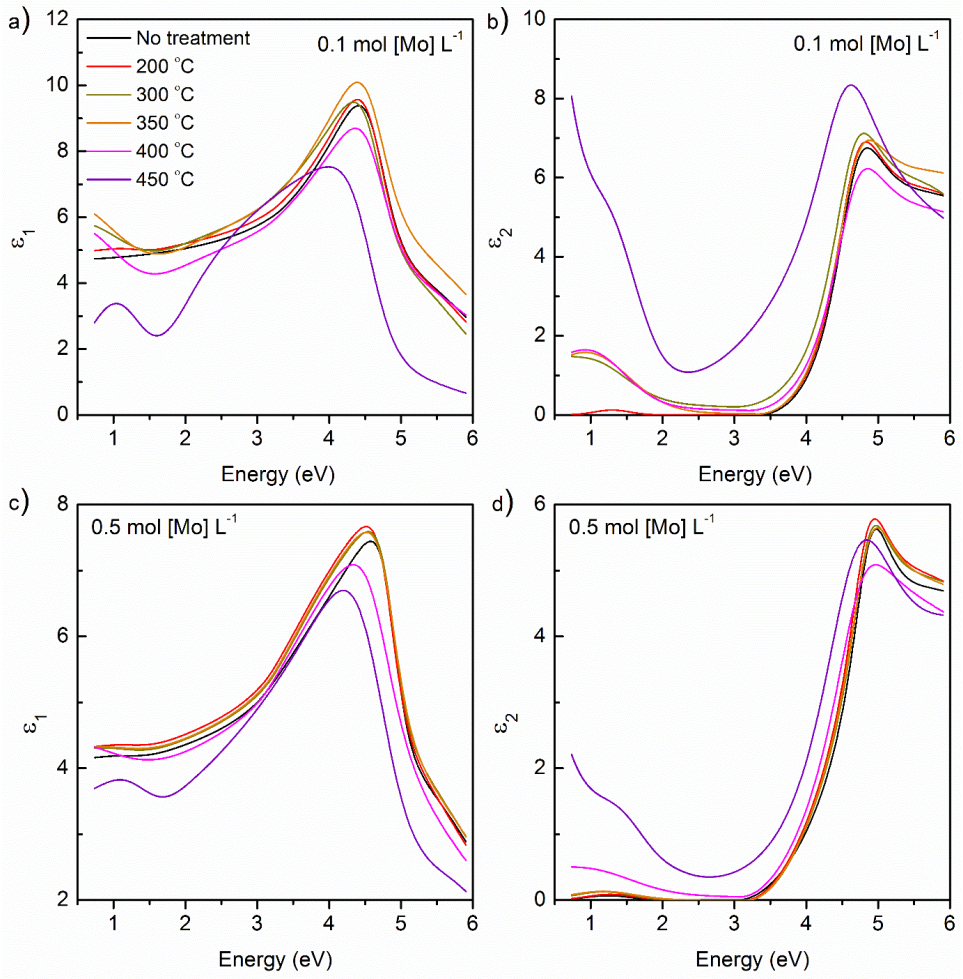

Figure 7. SE model of the real and imaginary parts of the dielectric function for the films from 0.1 mol [Mo] L^{-1} solution (a) and (b), and 0.5 mol [Mo] L^{-1} solution (c) and (d) after reduction in 5% H_2-95% Ar gas at 200, 300, 350, 400 and 450 °C, and films with no treatment in reducing gas.

Overall, the effect of reduction is greatly accelerated for the 0.1 mol [Mo] L^{-1} deposited films, with a greater proportion of reduced oxidation states. This occurs in combination with loss of material from the film, as seen by the decomposition of the film in Figure 5, suggesting that the mechanism of reduction differs with film thickness. With the denser alignment of nanocrystallites, there is better tolerance against loss of oxygen and loss of Mo species is prevented. The 0.5 mol [Mo] L^{-1} deposited film allows the incorporation of oxygen vacancies and development and growth of reduced molybdenum oxide phases without breakdown of film coverage. This should be considered when applying thin films of MoO_3 to devices: a thin and smooth film is often used in a sub-stoichiometric state, and although the morphology is favourable for low carrier recombination and lower resistivity, a discontinuous coverage may quickly occur. It is possible that the nanocrystalline plates allow fast diffusion of species into and out of the structure and correspondingly faster reduction kinetics. In contrast, the

thicker film morphology can provide a basis for well-developed reduced phases, which may also be enhanced by the layered structure.

4 Conclusions

A route to high quality, homogenous MoO_3 films with complete substrate coverage was demonstrated via deposition of monomeric molybdate species from aqueous solution. The amorphous as-deposited film crystallized by thermal annealing into a nanostructured arrangement of multicrystalline grains with ordering reflecting the layered crystal structure of MoO_3. The film morphology, including film thickness, grain size, and nanocrystallite orientation, was shown to be controlled by altering the solution concentration. As a consequence of the differing morphology, the kinetics and behaviours during reduction were modified. Films deposited from low concentration solution developed reduced phases at a lower temperature than films from a higher concentration solution, as determined by spectroscopic ellipsometry and X-ray photoelectron spectroscopy. However, these films with lower thickness exhibited film breakdown during reduction. In contrast, films deposited from higher concentration solution remained intact and allowed growth of new phases.

5 Acknowledgments

This work was performed within The Norwegian Research Centre for Solar Cell Technology project number 193829, a Centre for Environmentally-friendly Energy Research co-sponsored by the Research Council of Norway and research and industry partners in Norway. NTNU NanoLab is acknowledged for support and subsidized use of their facilities.

6 Declaration of interests

None.

7 References

1. Gaigneaux, E. M., Fukui, K. I. & Iwasawa, Y. Morphology of crystalline α-MoO_3 thin films spin-coated on Si (100). *Thin Solid Films* **374,** 49–58 (2000).

2. Meyer, J., Kidambi, P. R., Bayer, B. C., Weijtens, C., Kuhn, A., Centeno, A., Pesquera, A., Zurutuza, A., Robertson, J. & Hofmann, S. Metal Oxide Induced Charge Transfer Doping and Band Alignment of Graphene Electrodes for Efficient Organic Light Emitting Diodes. *Sci. Rep.* **4,** 5380 (2014).

3. Liu, J., Wu, X., Chen, S., Shi, X., Wang, J., Huang, S., Guo, X. & He, G. Low-temperature MoO_3 film from a facile synthetic route for an efficient anode interfacial layer in organic optoelectronic devices. *J. Mater. Chem. C* **2,** 158–163 (2014).

4. Battaglia, C., Yin, X., Zheng, M., Sharp, I. D., Chen, T., McDonnell, S., Azcatl, A., Carraro, C., Ma, B., Maboudian, R., *et al.* Hole Selective MoO_x Contact for Silicon Solar Cells. *NanoLetters* **14,** 967–971 (2014).

5. Xiang, D., Han, C., Zhang, J. & Chen, W. Gap States Assisted MoO_3 Nanobelt Photodetector with Wide Spectrum Response. *Sci. Rep.* **4,** 4891 (2014).

6. Hsu, C.-S., Chan, C.-C., Huang, H.-T., Peng, C.-H. & Hsu, W.-C. Electrochromic properties of nanocrystalline MoO_3 thin films. *Thin Solid Films* **516,** 4839–4844

(2008).

7. Alsaif, M. M. Y. A., Field, M. R., Murdoch, B. J., Daeneke, T., Latham, K., Chrimes, A. F., Zoolfakar, A. S., Russo, S. P., Ou, J. Z. & Kalantar-zadeh, K. Substoichiometric two-dimensional molybdenum oxide flakes: a plasmonic gas sensing platform. *Nanoscale* **6,** 12780–12791 (2014).

8. Brezesinski, T., Wang, J., Tolbert, S. H. & Dunn, B. Ordered mesoporous α-MoO_3 with iso-oriented nanocrystalline walls for thin-film pseudocapacitors. *Nat. Mater.* **9,** 146–151 (2010).

9. Ohtsuka, H. & Sakurai, Y. Characterization of MoO_{3-x} Thin Films. *Jpn. J. Appl. Phys.* **40,** 4680–4683 (2001).

10. Sinaim, H., Ham, D. J., Lee, J. S., Phuruangrat, A., Thongtem, S. & Thongtem, T. Free-polymer controlling morphology of α-MoO_3 nanobelts by a facile hydrothermal synthesis, their electrochemistry for hydrogen evolution reactions and optical properties. *J. Alloys Compd.* **516,** 172–178 (2012).

11. Hanlon, D., Backes, C., Higgins, T. M., Hughes, M., O'Neill, A., King, P., McEvoy, N., Duesberg, G. S., Mendoza Sanchez, B., Pettersson, H., *et al.* Production of Molybdenum Trioxide Nanosheets by Liquid Exfoliation and Their Application in High-Performance Supercapacitors. *Chem. Mater.* **26,** 1751–1763 (2014).

12. Shen, Y., Deng, S., Zhang, Y., Liu, F., Chen, J. & Xu, N. Highly conductive vertically aligned molybdenum nanowalls and their field emission property. *Nanoscale Res. Lett.* **7,** 463 (2012).

13. Shi, X.-B., Xu, M.-F., Zhou, D.-Y., Wang, Z.-K. & Liao, L.-S. Improved cation valence state in molybdenum oxides by ultraviolet-ozone treatments and its applications in organic light-emitting diodes. *Appl. Phys. Lett.* **102,** 233304 (2013).

14. Chiam, S. Y., Dasgupta, B., Soler, D., Leung, M. Y., Liu, H., Ooi, Z. E., Wong, L. M., Jiang, C. Y., Chang, K. L. & Zhang, J. Investigating the stability of defects in MoO_3 and its role in organic solar cells. *Sol. Energy Mater. Sol. Cells* **99,** 197–203 (2012).

15. Yang, W.-Q., Wei, Z.-R., Zhu, X.-H. & Yang, D.-Y. Strong influence of substrate temperature on the growth of nanocrystalline MoO_3 thin films. *Phys. Lett. A* **373,** 3965–3968 (2009).

16. Shafiei, M., Yu, J., Breedon, M., Motta, N., Wu, Q., Hu, Z., Qian, L., Kalantar-zadeh, K. & Wlodarski, W. Hydrogen Gas Sensors Based On Thermally Evaporated Nanostructured MoO_3 Schottky Diode: A Comparative Study. *IEEE Sensors* 8–11 (2011). doi:10.1109/ICSENS.2011.6126970

17. Goiz, O., Chávez, F., Felipe, C., Morales, N. & Peña-Sierra, R. Synthesis of molybdenum oxide microsheets via close-spaced vapor transport. *Mater. Sci. Eng. B Solid-State Mater. Adv. Technol.* **174,** 174–176 (2010).

18. Balendhran, S., Deng, J., Ou, J. Z., Walia, S., Scott, J., Tang, J., Wang, K. L., Field, M. R., Russo, S., Zhuiykov, S., *et al.* Enhanced Charge Carrier Mobility in Two-Dimensional High Dielectric Molybdenum Oxide. *Adv. Mater.* **25,** 109–114 (2013).

19. Li, Y. B., Bando, Y., Golberg, D. & Kurashima, K. Field emission from MoO_3

nanobelts. *Appl. Phys. Lett.* **81,** 5048–5050 (2002).

20. Navas, I., Vinodkumar, R. & Mahadevan Pillai, V. P. Self-assembly and photoluminescence of molybdenum oxide nanoparticles. *Appl. Phys. A* **103,** 373–380 (2011).

21. Li, F. & Chen, Z. Tuning electronic and magnetic properties of MoO_3 sheets by cutting, hydrogenation, and external strain: a computational investigation. *Nanoscale* **5,** 5321–33 (2013).

22. Haitao, X. & Xiang, Z. Investigation of hole injection enhancement by MoO_3 buffer layer in organic light emitting diodes. *J. Appl. Phys.* **114,** 244505 (2013).

23. Liang, J., Zu, F.-S., Ding, L., Xu, M.-F., Shi, X.-B., Wang, Z.-K. & Liao, L.-S. Aqueous solution-processed MoO_3 thick films as hole injection and short-circuit barrier layer in large-area organic light-emitting devices. *Appl. Phys. Express* **7,** 111601 (2014).

24. Rouhani, M., Foo, Y. L., Hobley, J., Pan, J., Subramanian, G. S., Yu, X., Rusydi, A. & Gorelik, S. Photochromism of amorphous molybdenum oxide films with different initial Mo^{5+} relative concentrations. *Appl. Surf. Sci.* **273,** 150–158 (2013).

25. Dasgupta, B., Ren, Y., Wong, L. M., Kong, L., Tok, E. S., Chim, W. K. & Chiam, S. Y. Detrimental Effects of Oxygen Vacancies in Electrochromic Molybdenum Oxide. *J. Phys. Chem. C* **119,** 10592–10601 (2015).

26. Sian, T. S. & Reddy, G. B. Optical, structural and photoelectron spectroscopic studies on amorphous and crystalline molybdenum oxide thin films. *Sol. Energy Mater. Sol. Cells* **82,** 375–386 (2004).

27. Lin, S.-Y., Chen, Y.-C., Wang, C.-M., Hsieh, P.-T. & Shih, S.-C. Post-annealing effect upon optical properties of electron beam evaporated molybdenum oxide thin films. *Appl. Surf. Sci.* **255,** 3868–3874 (2009).

28. Jasieniak, J. J., Seifter, J., Jo, J., Mates, T. & Heeger, A. J. A Solution-Processed MoO_x Anode Interlayer for Use within Organic Photovoltaic Devices. *Adv. Funct. Mater.* **22,** 2594–2605 (2012).

29. Fu, Q., Chen, J., Shi, C. & Ma, D. Room-Temperature Sol-Gel Derived Molybdenum Oxide Thin Films for Efficient and Stable Solution-Processed Organic Light-Emitting Diodes. *ACS Appl. Mater. Interfaces* **5,** 6024–6029 (2013).

30. Qiu, W., Hadipour, A., Müller, R., Conings, B., Boyen, H., Heremans, P. & Froyen, L. Ultrathin Ammonium Heptamolybdate Films as Efficient Room-Temperature Hole Transport Layers for Organic Solar Cells. *ACS Appl. Mater. Interfaces* **6,** 16335–16343 (2014).

31. Ho, P. Y., Sun, J. Y., Kao, S. H., Kao, C. Y., Lin, S. H., Lan, S., Tseng, W. H., Wu, C. I. & Lin, C. F. The effects of MoO_3 treatment on inverted PBDTTT-C:PC $_{71}$BM solar cells. *Sol. Energy Mater. Sol. Cells* **119,** 235–240 (2013).

32. Majhi, K., Bertoluzzi, L., Rietwyk, K. J., Ginsburg, A., Keller, D. A., Lopez-Varo, P., Anderson, A. Y., Bisquert, J. & Zaban, A. Combinatorial Investigation and Modelling of MoO_3 Hole-Selective Contact in $TiO_2|Co_3O_4|MoO_3$ All-Oxide Solar Cells. *Adv.*

Mater. Interfaces **3,** 1500405 (2016).

33. Diskus, M., Nilsen, O. & Fjellvåg, H. Growth of thin films of molybdenum oxide by atomic layer deposition. *J. Mater. Chem.* **21,** 705–710 (2011).

34. Liu, F., Shao, S., Guo, X., Zhao, Y. & Xie, Z. Efficient polymer photovoltaic cells using solution-processed MoO_3 as anode buffer layer. *Sol. Energy Mater. Sol. Cells* **94,** 842–845 (2010).

35. Murase, S. & Yang, Y. Solution Processed MoO_3 Interfacial Layer for Organic Photovoltaics Prepared by a Facile Synthesis Method. *Adv. Mater.* **24,** 2459–2462 (2012).

36. Tiwald, T. E., Thompson, D. W., Woollam, J. A., Paulson, W. & Hance, R. Application of IR variable angle spectroscopic ellipsometry to the determination of free carrier concentration depth profiles. *Thin Solid Films* **313–314,** 661–666 (1998).

37. Jellison Jr, G. & Modine, F. Parameterization of the optical functions of amorphous materials in the interband region. *Appl. Phys. Lett.* **69,** 371–373 (1996).

38. Fujiwara, H., Koh, J., Rovira, P. I. & Collins, R. W. Assessment of effective-medium theories in the analysis of nucleation and microscopic surface roughness evolution for semiconductor thin films. *Phys. Rev. B* **61,** 10832 (2000).

39. Johs, B. & Herzinger, C. M. Quantifying the accuracy of ellipsometer systems. *Phys. Status Solidi C* **5,** 1031–1035 (2008).

40. Aveston, J., Anacker, E. W. & Johnson, J. S. Hydrolysis of Molybdenum(VI). Ultracentrifugation, Acidity Measurements, and Raman Spectra of Polymolybdates. *Inorg. Chem.* **3,** 735–746 (1964).

41. Kihlborg, L. Least Squares Refinement of the Crystal Structure of Molybdenum Trioxide. *Ark. för Kemi* **21,** 357–364 (1963).

42. Borg, S., Liu, W., Etschmann, B., Tian, Y. & Brugger, J. An XAS study of molybdenum speciation in hydrothermal chloride solutions from 25-385°C and 600 bar. *Geochim. Cosmochim. Acta* **92,** 292–307 (2012).

43. Borgschulte, A., Sambalova, O., Delmelle, R., Jenatsch, S., Hany, R. & Nüesch, F. Hydrogen reduction of molybdenum oxide at room temperature. *Sci. Rep.* **7,** 40761 (2017).

44. Kennedy, M. J. & Bevan, S. C. A Kinetic Study of the Reduction of Molybdenum Trioxide By Hydrogen. *J. Less-Common Met.* **36,** 23–30 (1974).

45. Lalik, E., David, W. I. F., Barnes, P. & Turner, J. F. C. Mechanisms of Reduction of MoO_3 to MoO_2 Reconciled? *J. Phys. Chem. B* **105,** 9153–9156 (2001).

46. Bursill, L. A. Crystallographic shear in molybdenum trioxide. *Proc. R. Soc. Lond. A. Math. Phys. Sci.* **311,** 267–290 (1969).

47. Ivanova, T., Szekeres, A., Gartner, M., Gogova, D. & Gesheva, K. A. Spectroscopic characterization of CVD-molybdenum oxide films. *Electrochim. Acta* **46,** 2215–2219 (2001).

48. Szekeres, A., Ivanova, T. & Gesheva, K. Spectroscopic ellipsometry study of CVD molybdenum oxide films : effect of temperature. *J. Solid State Electrochem.* **7,** 17–20 (2002).

49. Arfaoui, A., Ouni, B., Touihri, S., Mhamdi, A., Labidi, A. & Manoubi, T. Effect of annealing in a various oxygen atmosphere on structural, optical, electrical and gas sensing properties of Mo_xO_y thin films. *Opt. Mater. (Amst).* **45,** 109–120 (2015).

50. Boukhachem, A., Kamoun, O., Mrabet, C., Mannai, C., Zouaghi, N., Yumak, A., Boubaker, K. & Amlouk, M. Structural, optical, vibrational and photoluminescence studies of Sn-doped MoO_3 sprayed thin films. *Mater. Res. Bull.* **72,** 252–263 (2015).

51. Kostis, I., Vourdas, N., Papadimitropoulos, G., Douvas, A., Vasilopoulou, M., Boukos, N. & Davazoglou, D. Effect of the Oxygen Sub-Stoichiometry and of Hydrogen Insertion on the Formation of Intermediate Bands within the Gap of Disordered Molybdenum Oxide Films. *J. Phys. Chem. C* **117,** 18013–18020 (2013).

52. Itoh, M., Hayakawa, K. & Oishi, S. Optical properties and electronic structures of layered MoO_3 single crystals. *J. Phys. Condens. Matter* **13,** 6853–6864 (2001).

53. Simchi, H., McCandless, B. E., Meng, T., Boyle, J. H. & Shafarman, W. N. Characterization of reactively sputtered molybdenum oxide films for solar cell application. *J. Appl. Phys.* **114,** 13503 (2013).

54. Mohamed, S. H., Kappertz, O., Ngaruiya, J. M., Pedersen, T. P. L., Drese, R. & Wuttig, M. Correlation between structure, stress and optical properties in direct current sputtered molybdenum oxide films. *Thin Solid Films* **429,** 135–143 (2003).

55. Inzani, K., Nematollahi, M., Vullum-Bruer, F., Grande, T., Reenaas, T. W. & Selbach, S. M. Electronic properties of reduced molybdenum oxides. *Phys. Chem. Chem. Phys.* **19,** 9232–9245 (2017).

56. Hamelmann, F., Brechling, A., Aschentrup, A., Heinzmann, U., Jutzi, P., Sandrock, J., Siemeling, U., Ivanova, T., Szekeres, A. & Gesheva, K. Thin molybdenum oxide films produced by molybdenum pentacarbonyl 1-methylbutylisonitrile with plasma-assisted chemical vapor deposition. *Thin Solid Films* **446,** 167–171 (2004).

57. Porter, V. R., White, W. B. & Roy, R. Optical Spectra of the Intermediate Oxides of Titanium, Vanadium, Molybdenum, and Tungsten. *J. Solid State Chem.* **4,** 250–254 (1972).

58. Inzani, K., Nematollahi, M., Selbach, S. M., Grande, T. & Vullum-Bruer, F. Progression of Reduction of MoO3 Observed in Powders and Solution-Processed Films. *Thin Solid Films* **626,** 94–103 (2017).